Transition Radiation Detector for the GlueX experiment

Alexander Austregesilo, Eugene Chudakov, Sergey Furletov, Kondo Gnanvo, and Lubomir Pentchev
Thomas Jefferson National Accelerator Facility, Newport News, Virginia 23606, USA

Volker Crede, Sean Dobbs, and Daniel Lersch
Florida State University, Tallahassee, Florida 32306, USA

Justin R. Stevens
College of William and Mary, Williamsburg, Virginia 23185, USA

(Dated: March 1, 2022)

Abstract

We propose to build a Transition Radiation Detector (TRD) with Gaseous Electron Multiplier (GEM) amplification, referred as GEM-TRD, to improve the electron-pion separation in the GlueX experiment. It will allow to study precisely reactions with electron-positron pairs in the final states; such reactions like J/ψ photoproduction near threshold have significant impact in many fields of the particle physics. The document discusses the motivation for such an upgrade and the physics goals, together with the technical description of the proposed detector and the electronics. Requirements for the GEM-TRD gas system are specified. Finally, estimates of the costs and the proposed time line are presented.

CONTENTS

I. EXECUTIVE SUMMARY

Important features of the GlueX detector include full acceptance, charge and neutral particle registration, precise knowledge of the photon beam energy, and high-rate electronics and DAQ, however it has limited particle-identification capabilities. A DIRC detector was built for the phase-II of the GlueX experiment and used for pion/kaon separation that will extend the GlueX program by including strangeness physics. Another important extension of the program would be the di-electron physics. The GlueX detector has the unique possibility to study the J/ψ photoproduction off the proton near threshold in the full kinematic space. As the J/ψ-proton interaction is mediated predominantly by gluons, such studies allow to probe the gluonic content of the proton: mass radius, anomalous contribution to the mass of the proton, the gluonic GPD; all these properties are not accessible with electromagnetic probes. First results of the J/ψ photoproduction near threshold [1], published by GlueX in 2019, collected already 100+ citations. The studied reaction $\gamma p \to pe^+e^-$ included the J/ψ decays and the Bethe-Heitler (BH) process, the latter was used for normalization of the cross section. Such studies require a good electron identification because of a huge pion background that can mimic the electron-positron pairs. In GlueX, the identification was provided by the electromagnetic calorimeters. Still, the selected sample of electron-positron pairs contained a considerable pion contamination, and the related uncertainties were the major contribution to the systematic errors.

The addition of the proposed Transition Radiation Detector (TRD) employing Gaseous Electron Multiplier (GEM) technology [2], or GEM-TRD, has the following advantages:

- As an independent low-mass detector, it can be placed in front of the electromagnetic calorimeter allowing to measure precisely the calorimeter's pion suppression efficiency, which is critical for the above studies. At the same time the calorimeter can be used to study the efficiency of the GEM-TRD.

- The proposed detector will give a factor of 10 pion suppression allowing to study the Bethe-Heitler (BH) electromagnetic process that is fully calculable and has the same e^+e^-p particles in the final state as the J/ψ photoproduction. This will reduce the

systematic uncertainties of the latter reaction significantly, e.g. for the total normalization from 27% to less than 10%.

- The detector will minimize the pion contamination in the J/ψ events to a level at which amplitude analysis can be performed reliably. The null results [1, 3] of the search in the J/ψ photoproduction for the LHCb pentaquarks [4, 5] mean that, if they exists, we have limited sensitivity. Therefore, amplitude analysis in the whole kinematic space might be crucial for identifying such states or setting much lower limits on their existence.

- The detector will allow measurements of the Dalitz decays of the lightest vector and pseudoscalar mesons giving access to the electromagnetic transition form factors (TFFs). Such studies play an important role in understanding the properties of these strongly interacting particles and, moreover, they are crucial for low-energy precision tests of the Standard Model (SM), in particular, to our understanding of the hadronic contributions to the anomalous magnetic moment of the muon.

- The ability to obtain high purity samples of di-electron events opens the possibility to study the Timelike Compton Scattering (TCS). Its interference with the BH process provides significant sensitivity to the GPDs through the extraction of Compton Form Factors (CFFs), similar to the DVCS process.

- The GEM-TRD works also as a Time Projection Chamber (TPC) giving a track segment within the drift volume of the detector. This will improve the pattern recognition and the momentum resolution which is limited in the forward direction and, at the same time, help the performance of the DIRC detector by providing it with a precise tracking just in its front.

The building of the GEM-TRD includes several stages: (1) measurements with small prototypes to prove the principle and make initial detector design (already finished), (2) manufacture and test a large-scale prototype (2021-2023 in progress), (3) design and produce a gas recirculating system (2022-2023), (4) manufacture one of the two chambers of the final detector and use it during the phase-II of the GlueX experiment (2023-2025), (5) manufacture the second chamber (2025-2026).

We estimate the total price of the full detector to be in the range of \$565−810k, depending on the electronics. If equipped with the flash ADCs that are used currently in the drift chambers of the GlueX experiment, we estimate a price of \$100 per channel, or \$490k for the whole electronics. Another option is to use a modern version of our electronics, that is now under development that may cut the price by a half.

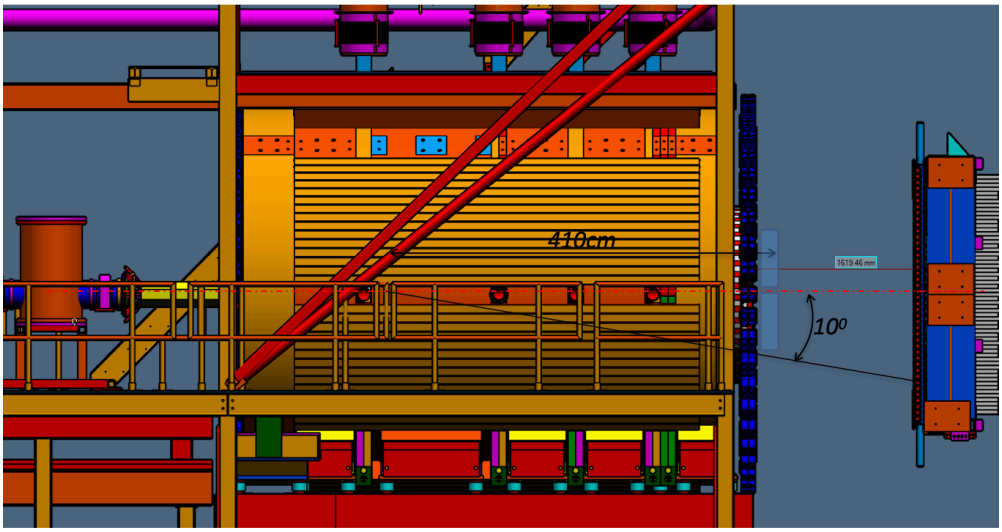

FIG. 1: Side view showing the approximate position of the proposed GEM-TRD detector (light blue boxes), at 410 cm downstream of the target, covering 86% of the forward GlueX acceptance of $\sim 10^{\circ}$ polar angle. The DIRC detector is not on the plot.

II. THE GEM-TRD DETECTOR

The proposed detector will be placed in the forward region of the GlueX detector just at the downstream face of the solenoid, in front of the DIRC and FCAL, see Figs. 1,2. It will consists of two separate chambers, each providing 1392×528 mm^2 sensitive area. The frames of the chambers holding the front-end electronics will be outside of the acceptance (Fig. 2).

The detector has a radiator layer 15 cm thick, followed by a 2 cm drift volume, and a GEM stage combined with a readout board. The principle of operation is illustrated in Fig.3a. The Transition Radiation (TR) photons in the keV region produced by the electrons in the radiator are absorbed by the Xe gas mixture in the drift volume emitting electrons that drift to and are amplified by the GEM. The signals are readout from X- and Y-strips on the readout board. The horizontal strips are separated in the middle and readout from the left and right side of the chambers (Fig. 2). The strip pitch is 1 mm, resulting in $2,448$ electronic channels per chamber, or $4,896$ in total. The signals are amplified on-board and

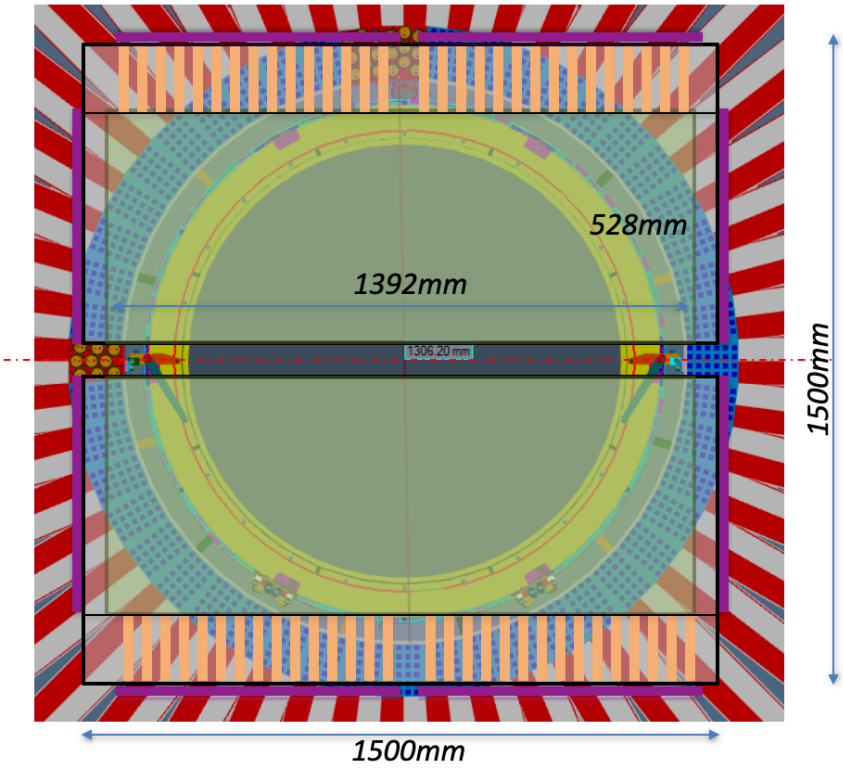

FIG. 2: Front view of the GEM-TRD detector placed at the face of the solenoid magnet. It consists of two separate chambers with 1392×528 mm^2 sensitive area. All the frames holding the front-end electronics (purple thick lines) of sizes $\sim 1500 \times 1500$ mm^2 are outside of the GlueX forward acceptance.

then digitized with flash ADCs. We assume using the same electronics as for the GlueX drift chambers: GASII [6] preamps and flashADC-125 [7], however alternative better and cheaper options will be discussed bellow. Thus we record the energy deposition along the track (measured by the drift time) that has different profile for the TR photons absorbed predominately at the entrance, and the track ionization that has uniform distribution, see Fig.3b. At the same time such detector works as a Time Projection Chamber, allowing to reconstruct the track segment within the drift volume.

The main parameters of the GEM-TRD detector are given in Table I. They are based on tests with small prototypes (10×10 cm^2) done during the past several years, as discussed in the next sections, and are preliminary. Further optimization of the detector will be done with a large-scale prototype that will be built and tested during the 2022 and 2023 running periods.

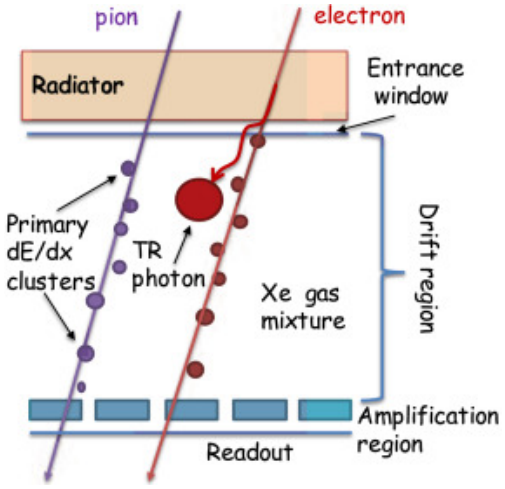

(a) GEM-TRD principle

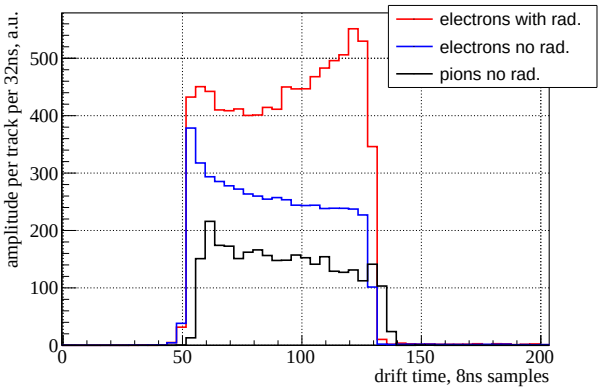

(b) Amplitude profiles for electrons with and without radiator and pions; data from studies with small prototypes

FIG. 3

parameter	value	comment
sensitive area	$2 \times (1392 \times 528\ \mathrm{mm}^2)$	two separate chambers
frame-free area	$1500 \times 1500\ \mathrm{mm}^2$	except some minimal support
distance from the target	4100 mm	
forward acceptance coverage	86%	for e^+e^- invariant mass > 1.2 GeV
radiator thickness	150 mm	
drift volume thickness	21 mm	
total detector thickness	$< 4\%$ R.L.	
drift field	1.5 kV/cm	
gas mixture	Xe/CO_2 90/10	
maximum drift time	800 ns	
gas amplification	$\sim 5.10^4$	
expected pion suppression factor	10	at 90% efficiency, based on studies with small prototypes
strip types	X and Y	on the same layer with capacitive coupling
strip pitch	1 mm	
x,y position resolution	150 μm	
z position resolution	250 μm	using drift time
readout channels	4,896	2,448 per chamber
GASII pre-amps (24 channels)	204	102 per chamber
GASII amplification	2.4 mV/fC	
flashADC-125 (72 channels)	68	34 per chamber
VXS crates	5	

TABLE I: Main parameters of the GEM-TRD detector.

III. PHYSICS OBJECTIVES

A. Improving the systematics of the J/ψ photoproduction using GEM-TRD

All the results in this subsection that illustrate the advantages of the GEM-TRD detector, are based on the data taken during the phase-I of the GlueX experiment. The phase-II of the experiment, that started initially in 2020, is planned continue in 2023-2024 and will accumulate in total a factor of ~ 5 more statistics. We anticipate to have at least half of the detector ready for this running period, thus having similar statistics (if not more) to the examples presented here.

The best approach to extract the absolute J/ψ cross-sections is to use the BH process for normalization using the formula [1]:

$$\sigma = \frac{N_{J/\psi}}{N_{BH}} \frac{\sigma_{BH}}{BR_{J/\psi}} \frac{\varepsilon_{BH}}{\varepsilon_{J/\psi}} , \tag{1}$$

where only the relative efficiency, $\varepsilon_{BH}/\varepsilon_{J/\psi}$, of the J/ψ and BH processes enters; here N_{BH} and $N_{J/\psi}$ are the yields of the corresponding processes, σ_{BH} – the calculated BH cross-section, and $BR_{J/\psi}$ – the branching ratio of the $J/\psi \to e^+e^-$ decay.

Fig.4 illustrates the problem with the pion background in the GlueX detector. It shows the e^+e^- invariant mass spectrum from the data (black), compared to simulations that include absolute calculations of the BH process [8–10] in the continuum and the J/ψ peak normalized to the data (blue). For this plot we apply all the selections as explained in [1]. Most importantly, 3σ cuts are applied around the peaks in the p/E distributions (p is the momentum and E the energy deposited in the corresponding calorimeter, BCAL and FCAL) for both, the electron and the positron candidates. Additional selection is applied on the signal from the first layer of BCAL, that works as a pre-shower. As we register all the final state particles and have very good precision for the beam photon energy, we can apply a Kinematic Fit (KF) that constrains the four momenta and the vertex position of the final state particles. The KF reduces significantly the background, as discussed below.

Thus, after all selections applied, the pion background is of the same order as the signal and, therefore, we have to use some statistical procedures to estimate the background and extract the BH yields. The result of such procedure is shown on the same plot – the red points in Fig.4 correspond to the simulations (blue) to which the pion background is added

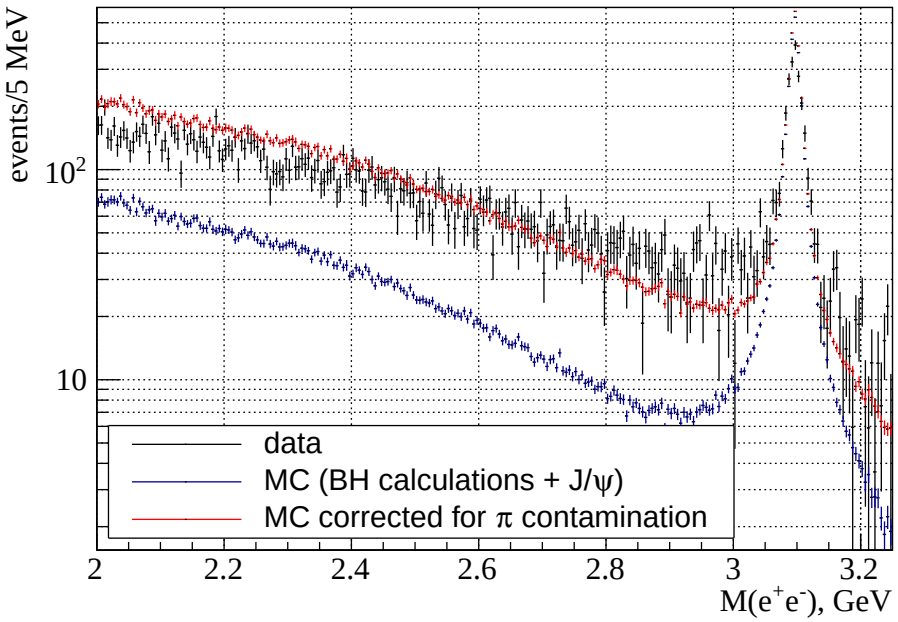

FIG. 4: The e^+e^- invariant mass spectrum from data compared to Monte Carlo simulations that use absolute BH calculations (as well as the J/ψ photoproduction normalized to the data) and their modification that adds the pion background (see text). The invariant mass was deduced from the kinematically fitted lepton momenta.

using the signal-to-background ratios in Figs.5a,5b. Examples of p/E fits used to estimate these ratios from the data are given in the Appendix.

In Fig.6 we plot the e^+e^- mass spectra for two cases, when at least one lepton goes forward and when both leptons are registered in the BCAL. The pion background is much more significant in the forward direction, where the GEM-TRD will be installed. This can be explained by the fact that background reactions like $\gamma p \to \Delta\pi \to p\pi\pi$ (Δ can be any other nuclonic resonance) will produce predominately one forward pion and one backward coming from the target excitation.

1. Pion rejection efficiency

The simulation of the calorimeter response is not perfect. Thus, the selections applied to data and simulations may have different efficiencies. At the same time, the p/E cuts are the most important in rejecting the pions. The fitting procedures to extract the e^+e^- yields are very sensitive to these selections and suffer from instability, especially for FCAL due to the steep background (see Appendix). One can try to do effective corrections to

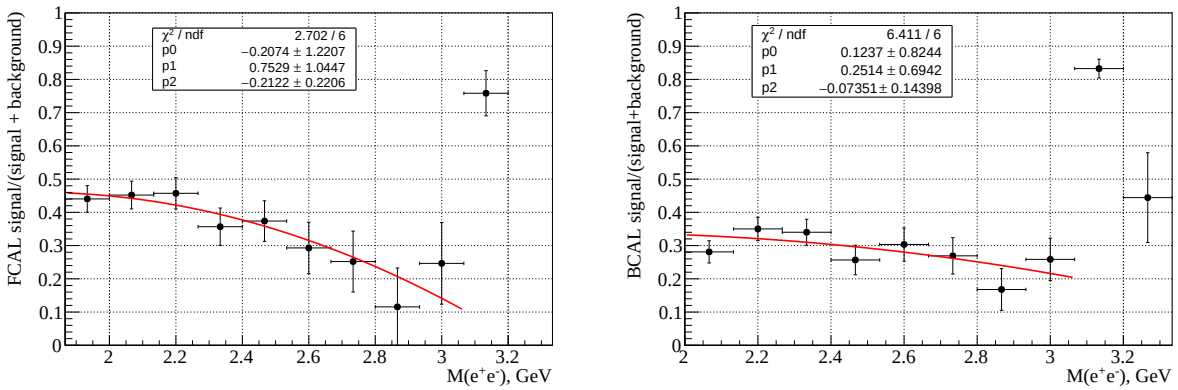

(a) FCAL (b) BCAL

FIG. 5: The signal to (signal+background) ratio as function of the e^+e^- invariant mass, obtained from p/E fits of the data, as explained in the Appendix. The results for the two calorimeters are fitted with polynomials, the latter used to add the pion background in Fig.4.

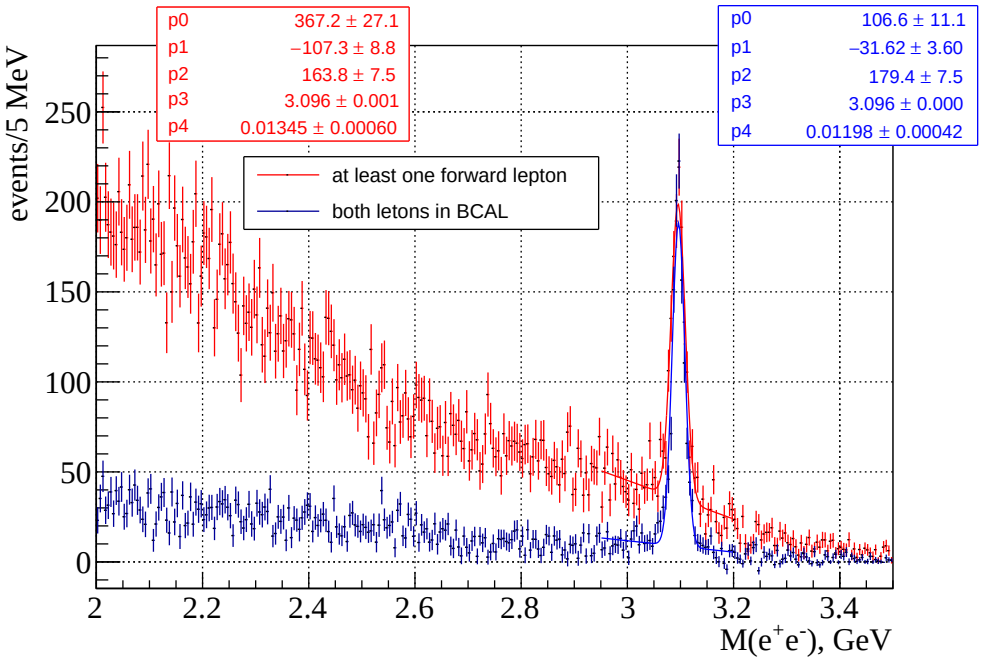

FIG. 6: The e^+e^- invariant mass spectrum from data in case of at least lepton goes in the forward direction, and when both leptons are registered in BCAL. The background below the J/ψ peak $\pm 3\sigma$ in forward direction is 65%.

the simulations based on the data, however, due to the momentum and angular dependence of these correction, this is not possible in practice. Therefore, so far, we were not able to attribute any systematic error related to the pion rejection efficiency. The best solution would be to use the GEM-TRD in front of the FCAL to create a clean sample of electrons

and measure the FCAL efficiency. For that we don't need the whole acceptance of the GlueX detector and propose to do such measurements, first, with one chamber only – see the timeline of the proposal in Sec.VII. Then, the results of these measurements can be used for the whole data set to improve the simulations and assign a realistic systematic error.

2. The efficiency of the Kinematic Fit

The Kinematic Fit (KF) cuts more than 50% of the final state particle candidates, therefore potentially it is a significant source of systematic errors. However, it is needed because it improves the e^+e^- mass resolution and reduces the background significantly, especially in the forward direction. As for the mass resolution, there is an alternative of using the measured electron/positron momenta and angles. Fig.7 shows the e^+e^- mass spectrum as measured by the missing mass off the recoil proton with and without the KF, in the case of at least one lepton in the forward direction. The mass resolution is as good as the standard reconstruction, however the background without the KF is significant and doesn't allow to extract the cross sections reliably, as the fluctuation of the background are similar in size to the J/ψ peak. Again, the use of the GEM-TRD would reduce the background to about 10% allowing to do studies with and without the KF and measure its efficiency.

3. BH normalization

Fig.8 compares the measured BH cross sections to the absolute calculations, as function of the invariant mass. One can see from Fig.8b that the data/MC ratio is not constant and shows a tendency of increasing towards the J/ψ peak, however with a significant uncertainty. Based on such studies we estimated [1] a contribution to the normalization uncertainty of about 25%, which is the dominant contribution to the systematics. We suspect that such data-MC inconsistency comes from the problems discussed in the previous subsections, the poor knowledge of the calorimeter and the KF efficiencies. In addition, we found that the errors of the cross section are dominated by the background fluctuations when fitting the p/E distributions (see Appendix).

If we assume negligible pion background, the errors will be significantly smaller as defined simply by the number of events, see Fig.9a. The individual errors of the data points in this

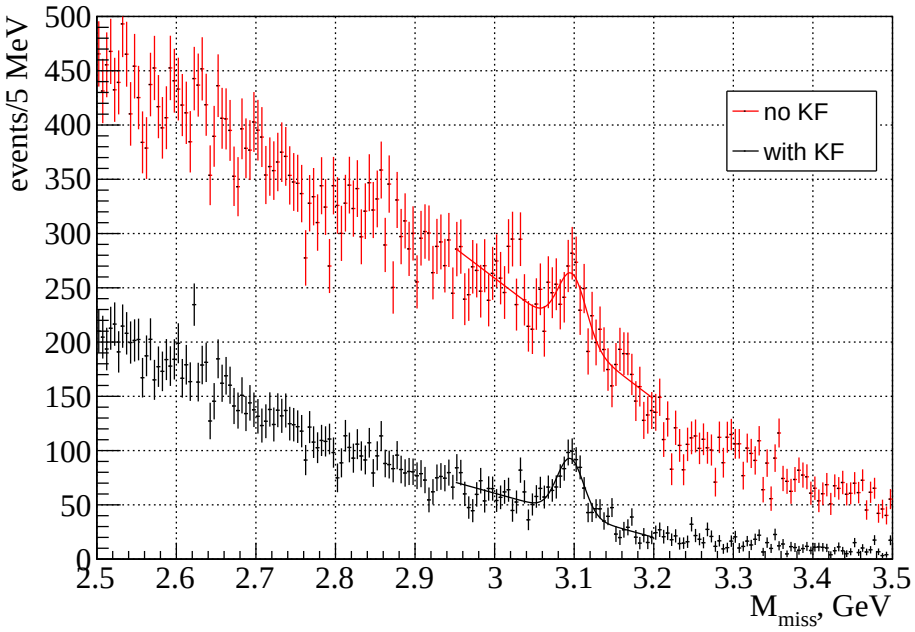

FIG. 7: The missing mass off the recoil proton from the data with and without Kinematic Fit (KF), with at least one forward lepton.

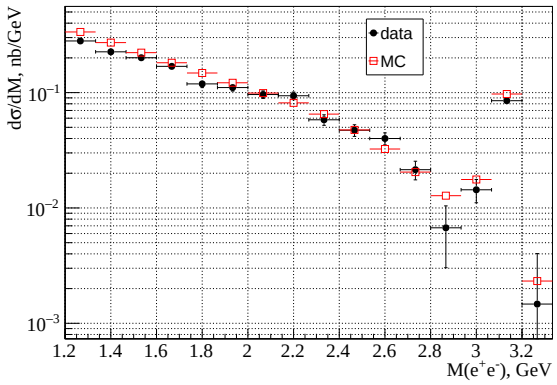

(a) BH cross-sections from data and MC.

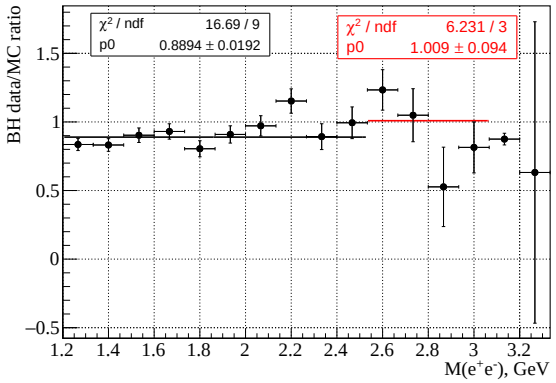

(b) BH data/MC ratio from Fig.8a fitted with constants in two regions.

FIG. 8: BH cross-section vs invariant mass: data vs MC.

case are given in Fig.9b and the fit in the region next to the J/ψ peak gives an uncertainty of 3%. Thus, when including all the contributions to the normalization error [1], the total normalization uncertainty would go down below 10%.

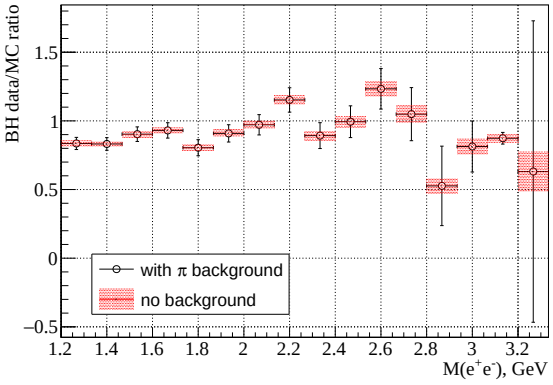

(a) Comparison of errors of the BH data/MC ratio with and without pion background.

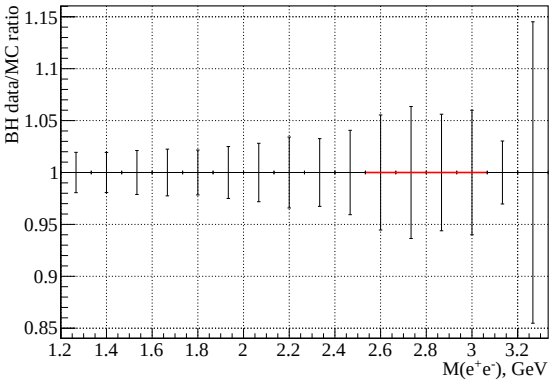

(b) The errors of the data points without background from Fig.9a (value set to unity). The fit with a constant of the points next to the J/ψ peak gives an error of 0.03.

FIG. 9

B. Amplitude Analysis of the J/ψ photoproduction and search for the LHCb pentaquarks

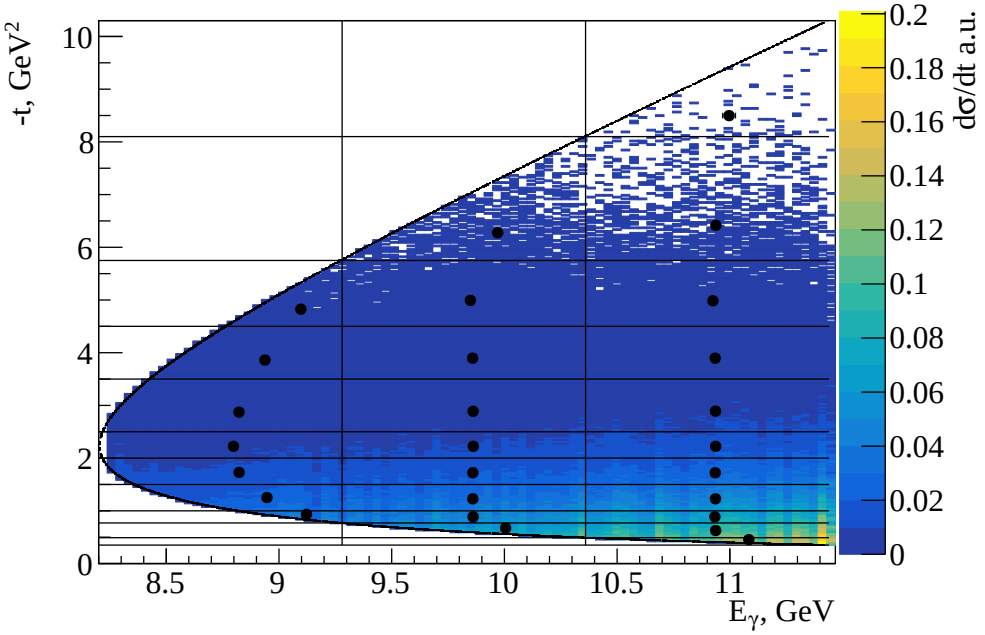

FIG. 10: The coverage of the kinematic space of the J/ψ photoproduction near threshold, with bins where GlueX will provide measurements of the $2D$ differential cross section. Shown are results from simulations, just for illustration.

If the LHCb pentaquarks [4, 5] exist, they should be seen in the s-channel of the J/ψ

photoproduction [11–13]. The negative results coming from JLab [1, 3] mean that indeed, if such states exist, we need more precise tools to identify them. The GlueX detector provides a uniform acceptance in the full kinematic range near the threshold where the pentaquarks are expected, see Fig.10. By detecting a resonant signal, the pentaquark interpretation of the states would be clearly distinguished from alternative explanations, e.g. nearby thresholds or dynamical effects in the three-body decay of the Λ_b, where these states were observed. A resonance is defined by a pole in the complex energy plane, which can only be properly established my measuring the amplitude for the process.

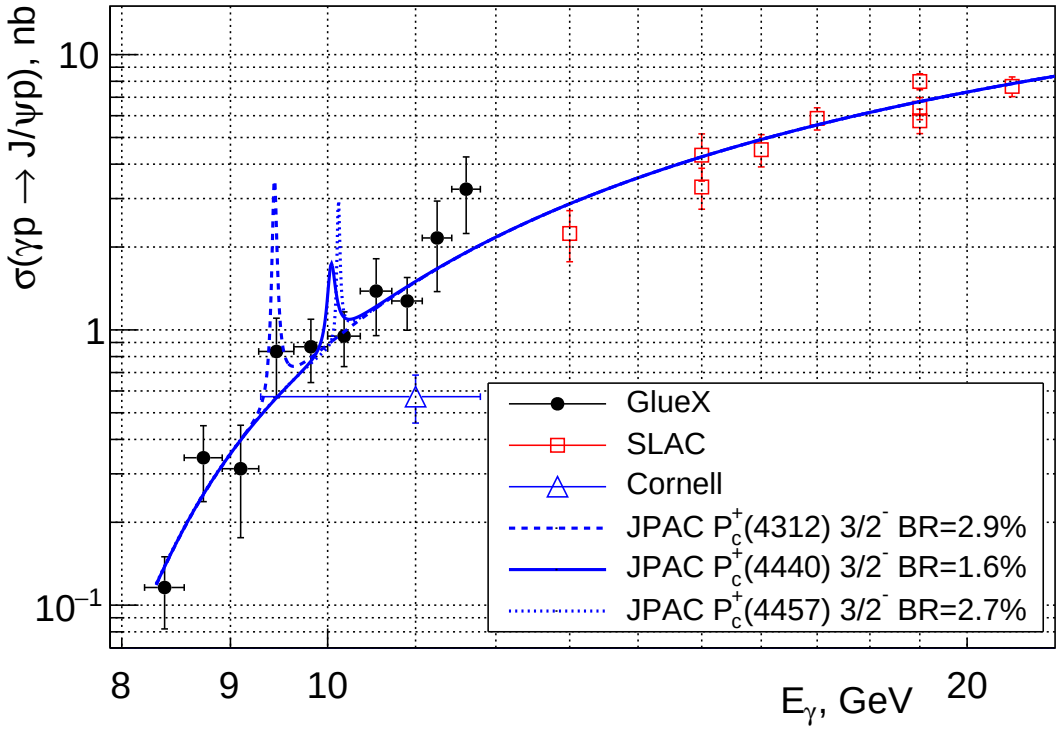

FIG. 11: GlueX results [1] for the J/ψ total cross-section vs beam energy, Cornell [14], and SLAC [15] data compared to the JPAC model [13] corresponding to $\mathcal{B}(P_c^+(4312) \to J/\psi p) = 2.9\%$, $\mathcal{B}(P_c^+(4440) \to J/\psi p) = 1.6\%$, and $\mathcal{B}(P_c^+(4457) \to J/\psi p) = 2.7\%$, for the $J^P = 3/2^-$ case.

With about 20% of the initial GlueX data, a few hundred events of J/ψ decaying into e^+e^- were reconstructed, where the electrons were identified by their electromagnetic showers in the calorimeters [1]. By using theoretical models for the $s-$channel production developed by JPAC [13], the GlueX collaboration was only able to extract model-dependent upper limits for the branching ratios of the charmed pentaquarks P_c from the energy-dependence of the

absolute cross section (cf. Figure 11). The full GlueX data set recorded to date provides more than one order of magnitude more reconstructed J/ψ events. An updated analysis of the total and differential cross sections does not have enough sensitivity to identify the pentaquarks in the spectrum.

An amplitude analysis of the angular distribution of the process will be necessary to uncover these elusive states. By using the full information from the kinematic distribution of the final state particles, interference between amplitudes can enhance very small signals and the phase acts as distinct signature. The linear polarization of the photon beam may increase the sensitivity in this regard even further [16]. This method will necessitate the selection of a clean signal sample, but with pions from hadronic interactions being more abundant than electrons by four orders of magnitude, the particle separation provided by the electromagnetic calorimeters is severely limiting the systematic uncertainties. The background is significant especially in forward direction, where it reaches 65% within 3σ of the J/ψ peak, see Fig.6. The GEM-TRD will reduce the pion contamination for the J/ψ events to about 5%, thus permitting a reliable amplitude description of the contributing reactions.

C. Light-meson Dalitz decays with GlueX

The study of the decays of the lightest vector $(\omega, \phi, ...)$ and pseudoscalar $(\eta, \eta', ...)$ mesons (M) into final states containing lepton pairs ($M \to \gamma^* B \to l^+ l^- B$, where B can be a photon or another meson) gives access to the electromagnetic transition form factors (TFFs). The latter play an important role in understanding the properties of these strongly interacting particles. Moreover, the study of these TFFs is also crucial for low-energy precision tests of the Standard Model (SM) and Quantum Chromodynamics (QCD). The theoretical description of the TFFs is relevant in our understanding of the hadronic contributions to the anomalous magnetic moment of the muon, where the uncertainties mainly originate from the hadronic vacuum polarization (HVP) and the hadronic light-by-light (HLbL) processes; in particular the $\omega \to 3\pi, \pi^0\gamma^*$ amplitudes contributing to both. Recently, data-driven approaches, using dispersion relations, have been proposed [17–19] that would make substantial and model-independent improvements to the determination of the HLbL contribution to $(g-2)_\mu$. The precision of the calculations used to describe the HLbL contributions can then be tested by directly comparing theoretical predictions from these approaches for the

TFFs of light mesons with experimental data.

Experimentally, the TFFs can be determined by measuring the actual decay rate of $M \to l^+l^- B$ as a function of the dilepton invariant mass $m_{ll} = q$, normalizing this dependence to the partial decay width $\Gamma(M \to B\,\gamma)$. GlueX has the potential to make important contributions to such studies, with its intense photon beam and large acceptance, but current measurements are limited by the existing electron identification capabilities. Fig. 12a shows the invariant mass of the $e^+e^-\gamma$ final state for a very small subset of the GlueX-I data, which already show some promising features: clear signals for $\pi^0 \to e^+e^-\gamma$ and $\eta \to e^+e^-\gamma$ are seen. While the decay rate of $\eta \to e^+e^-\gamma$ is suppressed by a factor of 10 compared to $\pi^0 \to e^+e^-\gamma$, and by an additional factor due to their different production cross sections, there are additional complications in identifying the η decay due to pion background coming primarily from $\rho \to \pi^+\pi^-$, being produced at a large rate in GlueX, combined with fake calorimeter signals. Additionally, there is a peaking background due to $\eta \to \pi^+\pi^-\gamma$ decays, which have a branching fraction an order of magnitude larger than that of $\eta \to e^+e^-\gamma$. Clearly, an increase of the pion rejection rate by a factor 10 would help to cleanly identify this reaction.

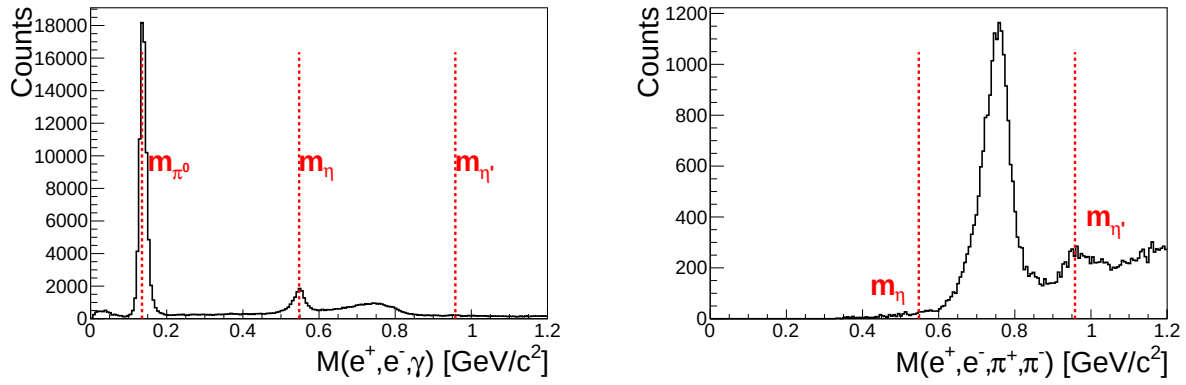

(a) $e^+e^-\gamma$ invariant mass

(b) $\pi^+\pi^-e^+e^-$ invariant mass

FIG. 12: Invariant mass of di-electron final states from $\approx 2\%$ of GlueX-I data. The vertical dashed lines indicate possible contributions for π^0, η and η'-mesons. The invariant mass was deduced from the kinematically fitted particle momenta.

The $\eta^{(\prime)} \to \pi^+\pi^-e^+e^-$ reactions can give information on the doubly-virtual TFFs, at the same time there are certain single photon transitions that are CP-forbidden. A possible CP-violating contributions to this reaction could be identified by measuring the asymmetry of the distribution of the opening angle Φ between the dipion and dilepton decay planes.

Fig. 12b shows the $\pi^+\pi^-e^+e^-$ invariant mass from a small fraction of the GlueX-I data. This mass plot indicates a $\eta' \to \pi^+\pi^-e^+e^-$ signal, sitting on top of a dominant $2(\pi^+\pi^-)$ background, which has been found to have a substantial cross section at GlueX with non-trivial structure. This background needs to be reduced by an improved lepton identification by at least an order of magnitude.

D. Timelike Compton Scattering

The ability to obtain high purity samples of di-electron events opens up other aspects of the JLab physics program in Hall D. Time-like Compton Scattering (TCS) [8], for example is time-reversal symmetric process to Deeply Virtual Compton Scattering (DVCS) which is studied extensively to probe the three-dimensional spatial structure of the proton at JLab and elsewhere. In TCS the incoming real photon produces a time-like high-Q^2 virtual photon which is observed as the di-lepton final state where the hard scale is set by the squared mass of the di-lepton pair where $M_{ee}^2 = Q^2$. While the TCS contribution is quite small, the interference with Bethe-Heitler provides significant sensitivity to the GPDs through the extraction of Compton Form Factors (CFFs), similar to the DVCS process.

Studies of TCS at JLab have already begun using quasi-real photons in CLAS12 from their Run Group A electron beam program [20]. Utilizing the unpolarized quasi-real photons the measurements agree with the predictions of GPD-based models, validating the application of this formalism to describe TCS data. Additional measurements in Hall D in the continuum of the e^+e^- invariant mass spectrum (Fig.4) could provide larger kinematic coverage than is accessible in CLAS12 and other observables utilizing the real linearly-polarized photon beam in Hall D [21].

E. Improving the tracking with the GEM-TRD

Important feature of the GEM-TRD detector is that it works also as a Time Projection Chamber (TPC), registering the clusters along the track in the drift volume as function of the drift time. Fig.13 illustrates how precise such tracking is; these results are from a test with a small prototype at the pair spectrometer arm (see Section IV). A tracking system that included the GEM-TRD prototype was installed and tested downstream of the solenoid

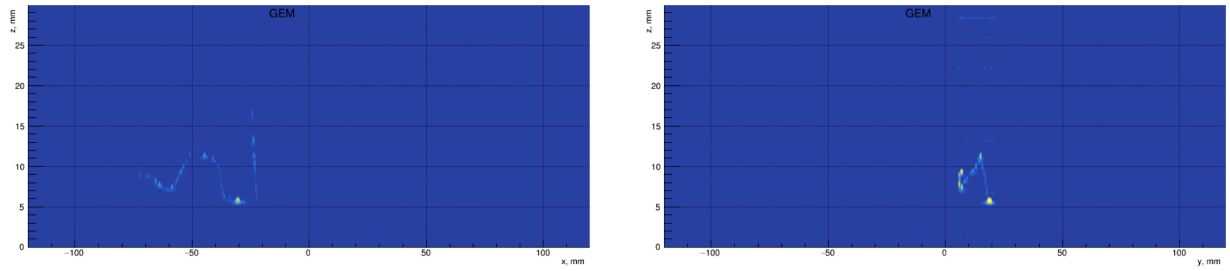

FIG. 13: One event reconstructed with GEM-TRD used as TPC: z vs x (left) and z vs y (right) where z is reconstructed from the drift time.

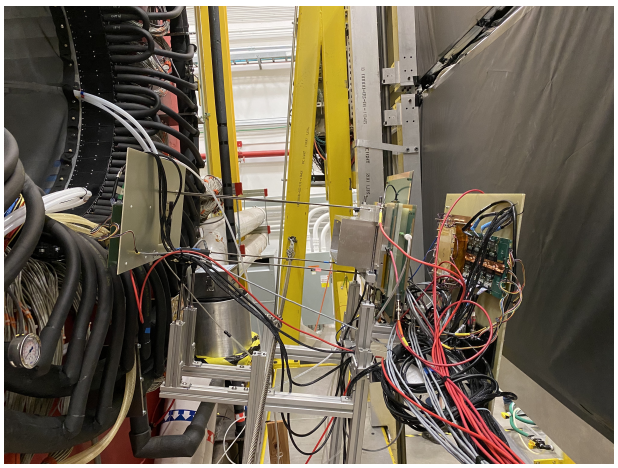

(a) GEM-TRD set-up installed downstream of the magnet (on the left) and in front of the DIRC detector (on the right). It includes pad GEM on the left, wire-TRD, and GEM-TRD on the right with front-end electronics and cables seen on the picture.

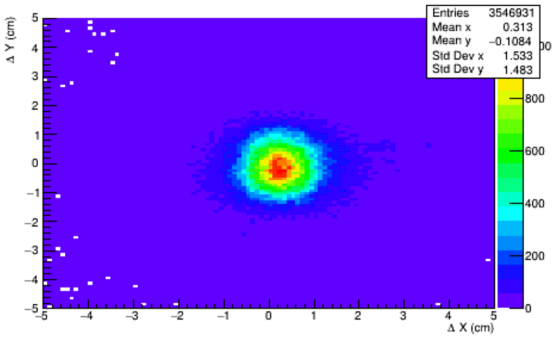

(b) Difference in x and y, between the track extrapolated from drift chambers and the track reconstructed in the GEM-TRD prototype downstream of the magnet.

FIG. 14

and in front of the DIRC detector (Fig.14a), just at the place where the final detector will be positioned. The tracks, as reconstructed from the drift chambers inside the magnet, are extrapolated to the GEM-TRD and compared with the tracks reconstructed there, Fig.14b. The GEM-TRD detector will add a tracking segment far away from the GlueX tracking system that has the potential to improve the pattern recognition and the momentum resolution in forward direction. At the same time, instead of using tracks extrapolated through the magnet's fringe field, the GEM-TRD will give a precise track just in front of the DIRC which is of critical importance for the reconstruction of the Cherenkov image in this detector.

IV. STUDIES WITH PROTOTYPES

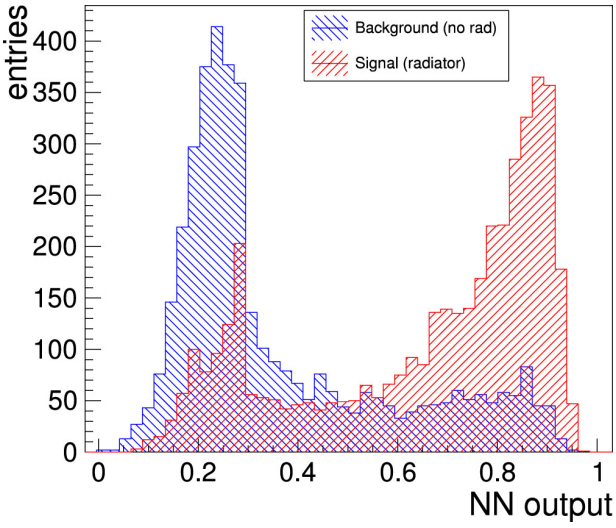

(a) Neural Network (NN) output for electrons with and without radiator

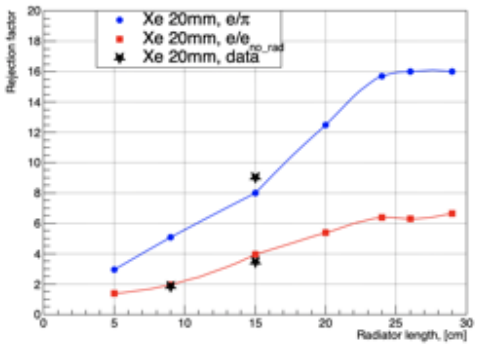

(b) Pion rejection factor from data (stars) and simulations, based on radiator/no radiator (red) and electron/pion (blue) comparison, as function of the radiator thickness. The data are from studies with small prototypes

FIG. 15

Studies with small ($10 \times 10\text{cm}^2$) prototypes have been done during 2018-2021 [2]. They were performed both with electrons, at one of the Pair Spectrometer arms, and with pions in the forward GlueX acceptance, downstream of the magnet and in front of the DIRC detector, see Fig.14a. Some results of these measurements were presented already in Sec.II, showing the timing profile of the detector response for electrons with/without radiator and for pions, Fig.3b. Event-by-event analyses using neural network were done (Fig.15a, Fig.15b) demonstrating a factor of ~ 4 effect of the radiator with electrons [2], and ~ 10 pion rejection factor, the later based on the experiments with electrons and pions done separately.

Such measurements proved the feasibility of using GEM technology for TR detectors. At the same time they helped to specify the parameters of next, large-scale prototype. This prototype will cover a quarter of the final detector (Fig.16), allowing to be used in real physics data taking. It will be produced under a contract with UVA that already started. We will use existing spare electronics to test it during 2022-2023.

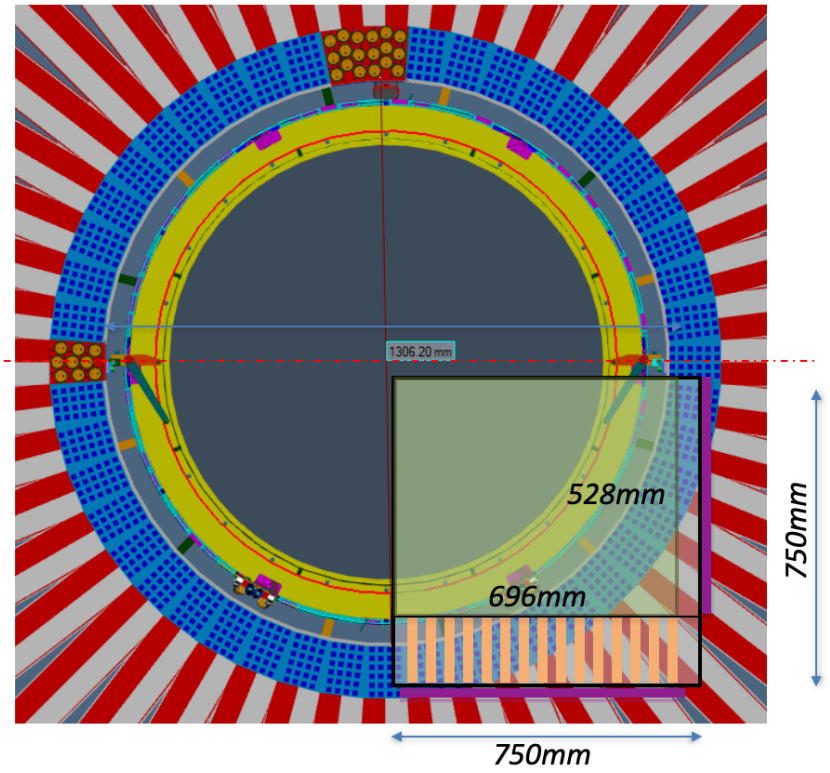

FIG. 16: Front view of the GEM-TRD large-scale prototype that has 696 × 528 mm^2 sensitive area.

V. GAS SYSTEM REQUIREMENTS

The high price of the Xe gas requires system that recirculates and purifies the gas mixture. The principle diagram of such system is shown in Fig.17. Each GEM-TRD module has two gas volumes - the main one filled with Xe/CO_2 gas mixture of 90/10% containing the drift and the amplification volumes, and the second one for the radiator filled with CO2. The thickness of the drift and amplification volume is 20 mm and 10 mm respectively. Thus, we estimate the Xe/CO_2 gas volume to be 25 l per chamber, or 50 l in total. For the CO_2 volume it has a thickness of 150 mm or 125 l per module and 250 l total. For the Xe/CO_2 volume we aim to have 8 volume exchanges per day, i.e. 20 l/h. The CO_2 volume can be exchanged once per day or 5 l/h.

The entrance and exit gas windows will be made of 100 μm Mylar, possibly enforced with Rochacell material. The detector will allow operation with overpressure between 0.5 and 2 mbar. The two gas volumes will be separated by 50 μm Mylar, covered with 1 μm Al. To limit the variations of the drift field, we require the pressure difference between the two gas

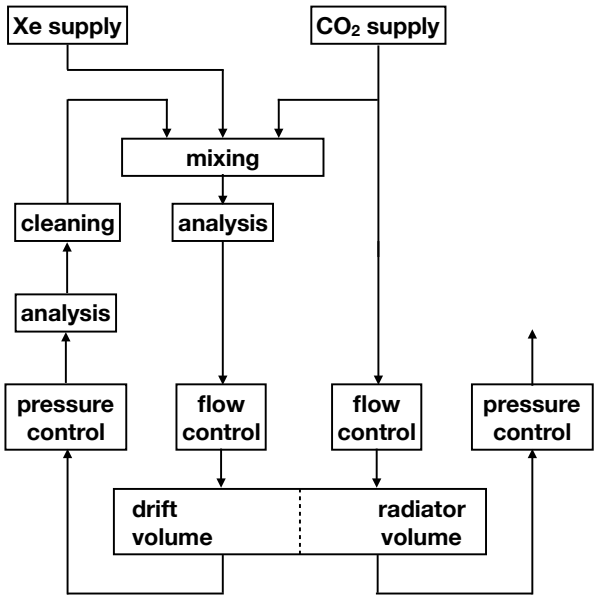

FIG. 17: Principle diagram of the gas recirculating system.

volumes to be less than 0.2 mbar.

Oxygen contamination and water vapor should be kept less than 50 ppm, to minimize the electron recombination in the drift volume. The Nitrogen contamination should be kept less than 0.5%.

The elements of the gas system that operate above 1 bar should be kept in a separate gas room, elevated approximately 7 m above the detector. They will be connected to the detector with gas lines of about 50 m length.

The parameters and requirements of the gas system are summarized in Table II.

item	requirement	comment
total Xe/CO_2 gas volume	50 l	
total CO_2 gas volume	250 l	
Xe/CO_2 gas flow	20 l/h	
CO_2 gas flow	5 l/h	
Operating overpressure	$0.5 - 2$ mbar	
Pressure difference b/n two volumes	< 0.2 mbar	
Oxygen contamination	< 50 ppm	
water vapor	< 50 ppm	
Nitrogen contamination	$< 0.5\%$	

TABLE II: General parameters and requirements for the GlueX TRD gas system.

VI. ELECTRONICS

We consider two options for the electronics. We can use the same electronics as for the GlueX drift chambers: GASII [6] preamps and flashADC-125 [7]. The fADC provides 125MHz sampling and standard readout in the GlueX DAQ. Based on a purchase made in 2015 for 25 fADC modules ($83/ch.), we assume for this option a price of $100 per channel.

The alternative of using the GlueX electronics is a high density and low power ($<$ 300 mW/chain) data acquisition (DAQ) system integrating 2240 readout channels inside a single OpenVPX crate [22, 23]. It is intended to be used in various applications, e.g. gaseous or scintillator-based particle detectors. It consists of 14 payload slots, controller, and data concentrator that communicate via multi-gigabit backplane. Each payload slot consists of a front module for digital and a rear transition module for analog processing. A pair of modules implements 160 full readout chains including amplification/shaping, sampling, and feature extraction. Sampling rate and ADC resolution are configurable for 80-1000 MS/s, and 14-8 bit, respectively. This electronics also provides a streaming readout and real time signal processing using neural network. The estimated cost per channel is about $50, i.e. half the price of the flashADC-125 [7]. The electronics is in the final stage of development and testing.

VII. COST ESTIMATES AND TIMELINE

The estimated cost for the whole detector is summarized in Table.III. It is dominated by the electronics and the two options discussed in the previous section are considered. The price of the detector itself is based on the contract for producing the large scale prototype, and the experience of building large GEM chambers. The gas system price was discussed with experts from CERN.

item	price, $k	comment
electronics, option 1 (4,900 channels)	490	using existing pre-amp and fADC
electronics, option 2 (4,900 channels)	245	using modern design, under development
design and manufacture two TRD chambers	120	
gas recirculating system	150	
mechanical support and infrastructure	50	
total option 1	810	
total option 2	565	

TABLE III: Cost estimate for the whole GEM-TRD detector for two electronics options.

The general timeline of the proposed GEM-TRD project is shown in Table.IV. The prototyping with small detectors proved the principle of using GEM technology for TR detectors and helped to formulate the specifications for the next large-scale prototype. A contract with UVA was signed to design and produce the large-scale prototype, that we intend to test during the 2022-2023 running periods. At the same time we plan to develop and produce the gas system. Based on the result with the large prototype we will finalize the detector design. The first chamber is planned to be manufactured and used during the phase-II of the GlueX experiment in 2023-2025. Even covering half of the acceptance, it will allow to measure the calorimeter efficiency and evaluate the KF, which results can be applied to the whole data set. In 2025-2026 we plan to produce second chamber and finish the project.

year	item	comment
2018-2021	tests with small prototypes	finished
2021-2023	produce and test large-scale prototype	in progress
2022-2023	design and produce gas system	
2023-2025	produce and evaluate one chamber	use during GlueX phase-II
2025-2026	produce and install the second chamber	

TABLE IV: General timeline of the GEM-TRD project.

[1] A. Ali et al. (GlueX collaboration), Phys. Rev. Lett. **123**, 072001 (2019).

[2] F. Barbosa, H. Fenker, S. Furletov, Y. Furletova, K. Gnanvo, N. Liyanage, L. Pentchev, M. Posik, C. Stanislav, B. Surrow, and B. Zihlmann, Nuclear Instruments and Methods in Physics Research Section A: Accelerators, Spectrometers, Detectors and Associated Equipment **942**, 162356 (2019).

[3] S. Joosten, Talk at 9th Workshop of the APS Topical Group on Hadronic Phtsics (2021).

[4] R. Aaij et al. (LHCb collaboration), Phys. Rev. Lett. **115**, 072001 (2015).

[5] R. Aaij et al. (LHCb collaboration), Phys. Rev. Lett. **117**, 082002 (2016).

[6] F. Babosa, https://halldweb.jlab.org/doc-private/DocDB/ShowDocument?docid=1364 The GAS-II/GPC-II GlueX Preamp Card Preliminary Test Results (2009).

[7] G. Visser, D. Abbot, F. Barbosa, C. Cuevas, H. Dong, E. Jastrzembski, B. Moffit, and B. Raydo, in *IEEE Nuclear Science Symposuim & Medical Imaging Conference* (IEEE, 2010) pp. 777–781.

[8] E. Berger, M. Diehl, and B. Pire, Eur.Phys.J.C **23**, 675 (2002).

[9] R. Paremuzyan, private communication (2017).

[10] R. Jones, private communication (2018).

[11] V. Kubarovsky and M. B. Voloshin, Phys. Rev. D **92**, 031502 (2015).

[12] M. Karliner and J. Rosner, Phys. Lett. B **752**, 329 (2016).

[13] A. Blin, C. Fernandez - Ramirez, A. Jackura, V. Mathieu, V. Mokeev, A. Pilloni, and A. Szczepaniak, Phys. Rev. D **94**, 034002 (2016).

[14] B. Gittelman, K. M. Hanson, D. Larson, E. Loh, A. Silverman, and G. Theodosiou, Phys. Rev. Lett. **35**, 1616 (1975).

[15] U. Camerini, J. Learned, R. Prepost, C. Spencer, D. Wiser, W. Ash, R. L. Anderson, D. M. Ritson, D. Sherden, and C. K. Sinclair, Phys. Rev. Lett. **35**, 483 (1975).

[16] D. Winney, C. Fanelli, A. Pilloni, A. . I. H. Blin, C. Fernndez-Ramrez, M. Albaladejo, V. Mathieu, V. . I. Mokeev, and A. . I. Szczepaniak, Phys. Rev. D **100** (2019).

[17] G. Colangelo et al. , Phys. Lett. B **738**, 6 (2014).

[18] G. Colangelo, M. Hoferichter, M. Procura, and P. Stoffer, JHEP **09**, 074 (2015).

[19] V. Pauk and M. Vanderhaeghen, Phys. Rev. D **90**, 113012 (2014).

[20] P. Chatagnon, S. Niccolai, S. Stepanyan, M. J. Amaryan, G. Angelini, W. R. Armstrong, H. Atac, C. Ayerbe Gayoso, N. A. Baltzell, L. Barion, M. Bashkanov, M. Battaglieri, I. Bedlinskiy, and et al., Physical Review Letters **127** (2021), 10.1103/physrevlett.127.262501.

[21] S. Pisano, A. Biselli, S. Niccolai, E. Seder, M. Guidal, M. Mirazita, K. P. Adhikari, D. Adikaram, M. J. Amaryan, M. D. Anderson, S. Anefalos Pereira, H. Avakian, J. Ball, and et al., Physical Review D **91** (2015), 10.1103/physrevd.91.052014.

[22] L. Jokhovets et al. , in *IEEE Transactions on Nuclear Science*, Vol. 61 (IEEE, 2014) pp. 3627–3634.

[23] L. Jokhovets, https://indico.gsi.de/event/12240/contributions/51989/attachments/35049/46047/DAQ_implementation_jokhovets.pdf DAQ FOR PANDA STT, IMPLEMENTATION (2020).

VIII. APPENDIX

Examples of the p/E fits in bins of the e^+e^- invariant mass are given in Fig.18 for BCAL and in Fig.19 for FCAL.

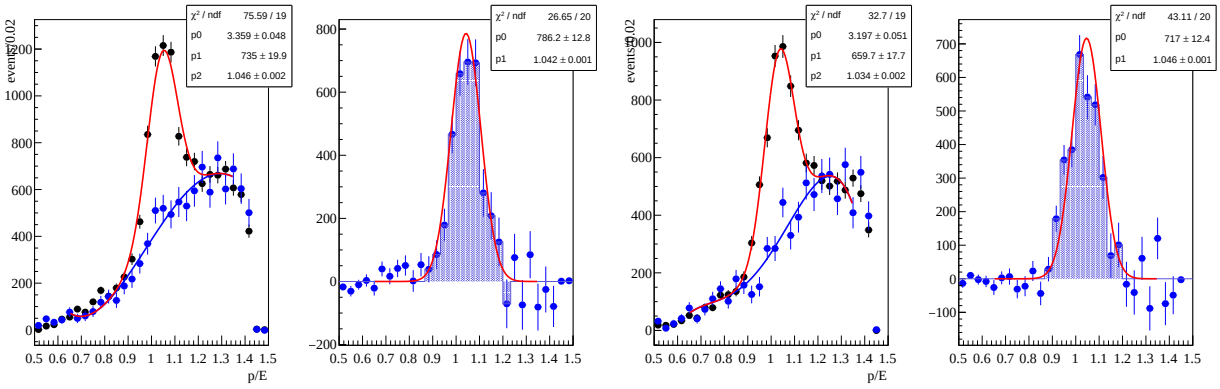

(a) BCAL $1.73 < M(e^+e^-) < 2$ GeV

(b) BCAL $2 < M(e^+e^-) < 2.27$ GeV

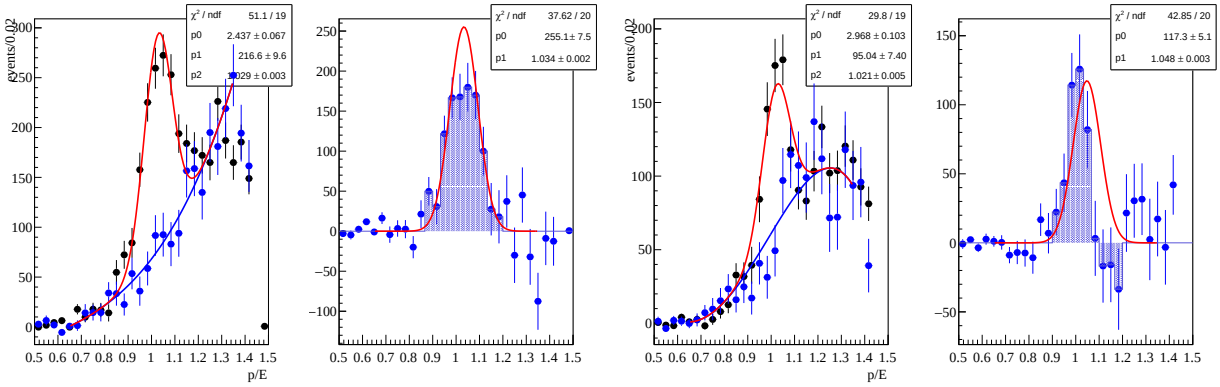

(c) BCAL $2.53 < M(e^+e^-) < 2.8$ GeV

(d) BCAL $2.8 < M(e^+e^-) < 3.07$ GeV

FIG. 18: Fits of p/E distributions for BCAL for four bins in $M(e^+e^-)$. In the left panel of each plot the blue points fitted with the blue curve represent the background distribution (from the sideband of the p/E distribution of the other lepton), while the total distribution is shown with black points fitted with a Gaussian (fixed σ) plus the background polynomial (p0-p4 parameters); the three fitted parameters are the normalization coefficients of the Gaussian and the polynomial and the mean of the Gaussian. The right panel is the difference between the black and blue points from the left panel, fitted with a Gaussian with fixed width (p0, p1 - amplitude and mean); the sum of the shaded points ($\pm 3\sigma$) is used as an estimate of the signal.

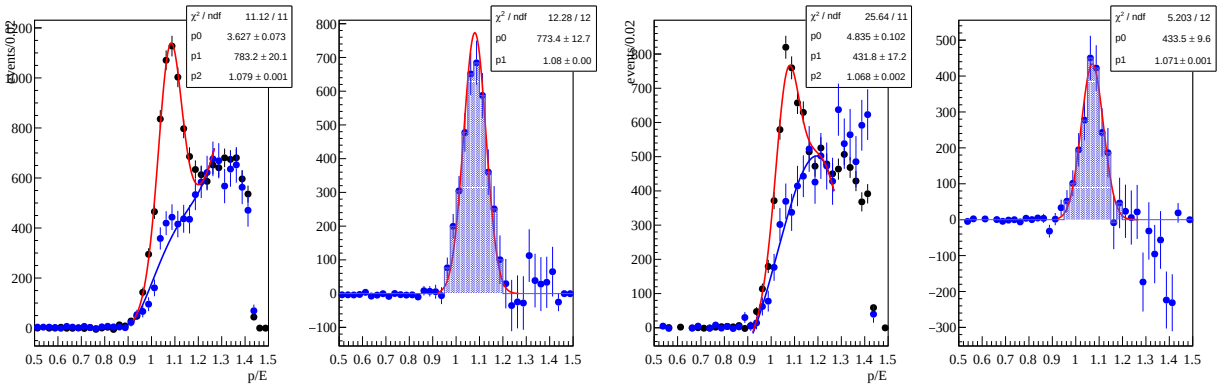

(a) FCAL $1.73 < M(e^+e^-) < 2$ GeV

(b) FCAL $2 < M(e^+e^-) < 2.27$ GeV

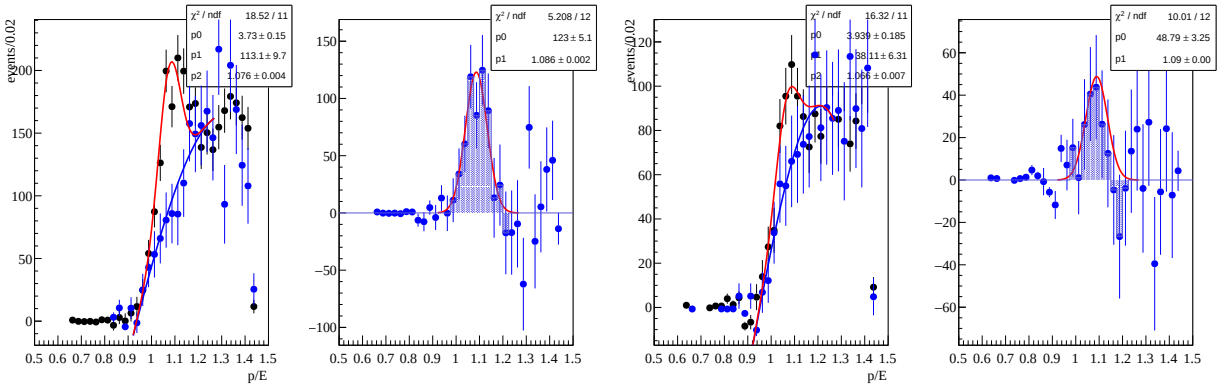

(c) FCAL $2.53 < M(e^+e^-) < 2.8$ GeV

(d) FCAL $2.8 < M(e^+e^-) < 3.07$ GeV

FIG. 19: Same as in Fig.18 but for FCAL.